NANO LETTERS

pubs.acs.org/NanoLett Letter

Delocalization of Quasiparticle Moiré States in Twisted Bilayer hBN

Arsineh Apelian, Annabelle Canestraight, Songyuan Liu, and Vojtěch Vlček*

Cite This: *Nano Lett.* 2024, 24, 11882–11888 Read Online

ACCESS | Metrics & More | Article Recommendations | Supporting Information

ABSTRACT: Twisted bilayers host many emergent phenomena in which the electronic excitations (quasiparticles, QPs) are closely intertwined with the local stacking order. By inspecting twisted hexagonal boron nitride (t-hBN), we show that nonlocal long-range interactions in large twisted systems cannot be reliably described by the local (high-symmetry) stacking and that the band gap variation (typically associated with the moire excitonic potential) shows multiple minima with variable depth depending on the twist angle. We investigate twist angles of 2.45°, 2.88°, 3.48°, and 5.09° using the GW approximation together with stochastic compression to analyze the QP state interactions. We find that band-edge QP hybridization is suppressed for intermediate angles that exhibit two distinct local minima in the moire potential (at AA region and saddle point (SP)) which become degenerate for the largest system (2.45°).

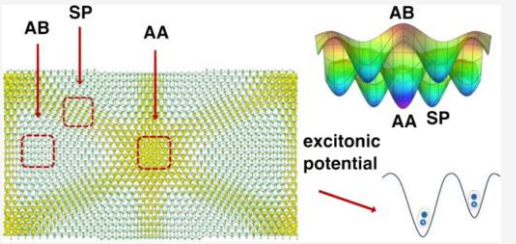

KEYWORDS: *hexagonal boron nitride, twisted bilayers, moire excitons, Dyson orbitals*

Twisted van der Waals structures have attracted considerable attention in the past decade.[1−5] These systems, composed of nominally weak monolayers, exhibit strongly correlated behavior[6,7] and harbor strongly localized excitations (quasiparticles - QPs; i.e. charged electrons, holes, or excitons), subject to a periodic potential landscape whose energy and spatial distribution are determined by the twist angle. It is widely recognized that the moiré superlattice can modulate the electronic band structure[8] and exhibit emergent properties such as unconventional superconductivity[9] and insulating behavior driven by correlations.[10−12] Similar new quantum phases are predicted for twisted bilayers of hexagonal boron nitride (t-hBN),[13−15] transition-metal dicalcogenides (TMD),[16−22] or phosphorene (t-BP).[23−27]

Guiding the development of moiré platforms necessitates a quantitative theoretical understanding of their properties. Commonly, they are derived from the local arrangements that are conveniently represented by the parent ("high-symmetry") structures. The QPs in such bilayers are subject to a local potential landscape formed by the distinct stacking orders in the 2D lattice. This is invoked in the description of effective excitonic potentials based on the local band gaps (i.e., local differences between QP energies of an electron and a hole).[28−31] Experiments show that by optically exciting the localized moiré states can generate strong interactions between electrons and holes, making them act as deep potential wells for excitons.[32−35] Here, the exciton is typically described as a QP moving through a slowly varying potential energy landscape which is often characterized by the variation of the local band gaps because the band-edge energy changes with the local geometry of the moiré superlattice.[28,29,36]

The extent of the nonlocal long-range interactions and effect on the individual QPs in the moiré potential is debated, given that localization is further aided through lattice distortions, enhancing the "trapping" of electronic states.[37] First-principles calculations of the twisted systems require large supercells with thousands of atoms and are thus typically limited to mean-field methods. Recent efforts in many-body perturbation theory (MBPT) focus on reconstructing the correlations from calculations of the parent systems[36−39] and rely on mean-field orbitals. To our knowledge, the only QP (Dyson) orbital reconstruction was so far achieved with stochastic methods for the correlated subspace in twisted bilayer graphene.[40] Moreover, the role of nonlocal correlations in the spatial extent of Dyson orbitals and their hybridization is unknown.

We overcome these limitations and investigate the QP landscapes by employing the *GW* approximation in the stochastic MBPT formulation.[41,42] To study the moiré states, we extend the technique to determine the Dyson orbitals from a stochastic compression of the orbital basis.[43] We explore the QP energy variation within the moiré lattice and the hybridization of the orbitals for t-hBN whose electronic structure is well described by *GW*[44] where the nonlocal correlation effects are considered and thus include weak (van der Waals) interlayer interactions. Further, calculations reveal the formation of flat bands and strong spatial localization of electrons at small twist angles.[13] Experiments also confirm excitonic states in t-hBN.[45]

Received: June 28, 2024
Revised: September 5, 2024
Accepted: September 6, 2024
Published: September 16, 2024

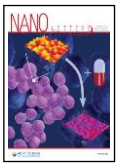

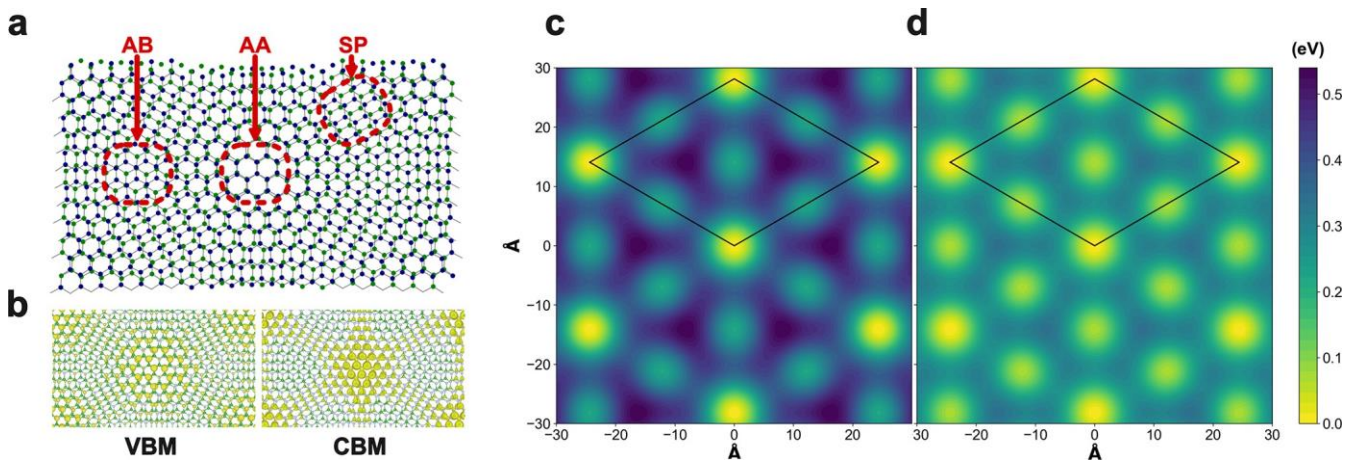

Figure 1. a) Structure of t-hBN with a twist angle of 5.09° showing the high-symmetry regions in dashed red boxes (AA, AB, SP). b) LDOS for the states near the valence band maxima (VBM) and conduction band minima (CBM) showed as a density isosurface in yellow using DFT. c) Local band gap variation (computed with s-G_0W_0 for θ = 5.09°) translated to a moiré potential heatmap constructed from the local environments based solely on the high-symmetry stacking regions. The deep minima correspond to the AA region (set to zero on the heat map scale); the moiré unit cell is shown for comparison. d) Moiré potential constructed from the LDOS projection computed for the entire twisted system shows much weaker local variations compared to the local approximation in c).

Here, we consider four small twist angles: 2.45°, 2.88°, 3.48°, and 5.09°, with structures containing up to ≈18,000 electrons. Our results reveal how localized moiré states hybridize due to a nontrivial interplay between local structure and nonlocal correlations. We compare the band gaps obtained independently for the individual high-symmetry structures with those performed on the entire t-hBN system, evaluated using the localized orbitals in various regions of the bilayer. The latter shows significantly reduced spatial variations, with the differences between adjacent low-gap regions (valleys) decreasing by almost an order of magnitude. For most twist angles, the nonlocal interactions lead to band-edge QP state mixing (hybridization), which is suppressed for intermediate angles. This behavior is mostly determined by the strength of interactions and localization in high-symmetry regions of the moiré cell. Most importantly, the calculations for the twisted systems reveal that the local excitonic potential is significantly decreased in the SP stacking region, leading to a characteristic "double well" that could potentially confine two types of moiré excitons.

t-hBN, a wide band gap semiconductor,[46] has a honeycomb-like structure and periodicity on the nm scale. Unlike other systems (e.g., TMD's[47−51]), it exhibits negligible spin−orbit coupling (SOC) and serves as a simple parent material to investigate at what extent can one approximate the moiré potential according to only the local environments and when it becomes necessary to consider fully twisted structures.

To disentangle the role of nonlocal correlations (stemming from density−density fluctuations) and the local structural arrangements, we first consider the electronic structure of the full moiré system and compare it to results for untwisted structures based on the high-symmetry stackings. The influence of atomic relaxations in twisted bilayers has been studied extensively where its been shown to play a role in many structural and electronic properties.[52−54] However, we deliberately construct noncorrugated (flat) bilayers in which the QP localization is driven by the potential variations due to the atomic position mismatch in the two layers. Here, we investigate the electronic contributions to QP localization, as opposed to distortion-assisted trapping of electronic states, which will further contribute to the localization of electronic states and, therefore, impact the exciton dynamics and binding energy in the moiré superlattice.[37]

Three high-symmetry points (AA, AB, SP) are identified as depicted in Figure 1(a), and twist angles of 2.45°, 2.88°, 3.48°, and 5.09° are considered. First, first-principles calculations based on density functional theory (DFT) are performed in a real-space implementation to study how the electronic states and band gaps are impacted by the interactions in twisted systems and explore the spatial distribution of the charge density in the band-edge states (i.e., the local density of states (LDOS)), constructed from a set of nearly degenerate electronic states which connect the relevant high-symmetry points (all those are within ∼140 meV for valence and ∼100 meV for conduction states) at the DFT level. We separate the states corresponding to the individual stacking regions by their spatial distributions. The degenerate edge states at the valence band show AA localization shown in Figure 1(b)(left), which is in agreement with previous works.[55] Energetically more distant valence states exhibit localization in the immediate neighborhood of AA, and deeper states span AB and SP regions (see Figure S.3). For the conduction band, the degenerate band-edge states (up to ∼100 meV) exhibit hybridization of two different stacking regions where electrons are localized in both the AA and SP regions shown in Figure 1(b)(right). Already at this point, the calculation for the entire t-hBN exhibits states delocalized between two high-symmetry points, which are missed when only local stacking orders are considered.

Despite the hybridization, we define the local band gaps by associating them with the transitions between the electronic states that are localized in the corresponding high-symmetry regions (i.e., relating the LDOS and QP energies). We compare these results to those obtained from the calculations for untwisted parent structures. We first employ the common "one-shot" perturbative correction, stochastic G_0W_0,[41,42] to the DFT eigenvalues. The computed G_0W_0 band gaps for t-hBN opens up to roughly the experimental value of approximately 6 eV[56,57] (depending on the particular twist angle or stacking). Full results (including DFT) for each region can be found in

https://doi.org/10.1021/acs.nanolett.4c03030
Nano Lett. 2024, 24, 11882−11888

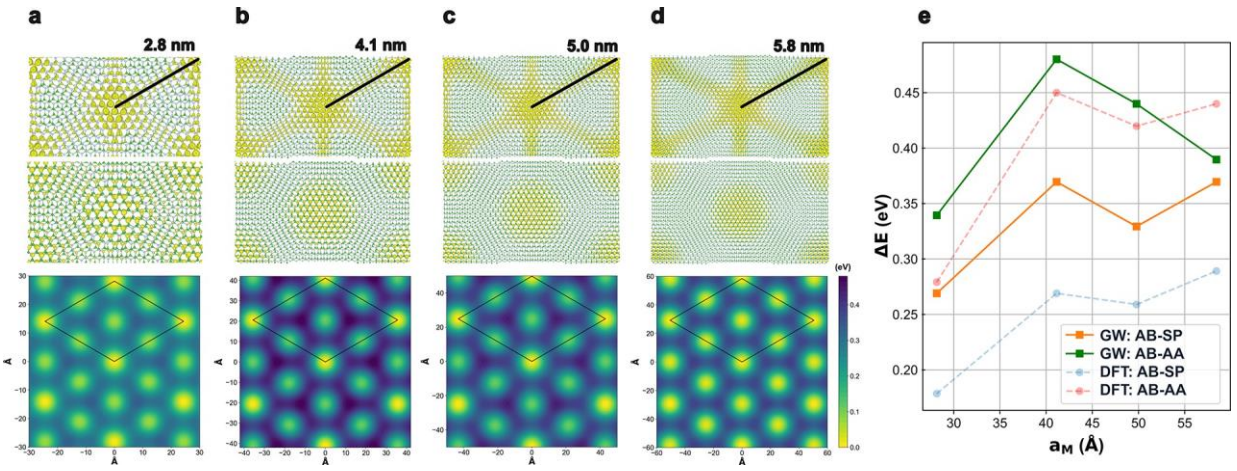

Figure 2. Plotted LDOS of the CBM (top) and VBM (bottom) obtained from DFT, and the corresponding moiré potentials computed with s-G_0W_0 for twist angles of a) 5.09°, b) 3.48°, c) 2.88°, and d) 2.45°. The zero of the moiré potential is set at the minimal local gap in the AA stacking region (yellow on the heat map). The moiré unit cell is shown for each plot by black lines with vertices in the AA region. At 3.48°, the system shows weak secondary minima in the SP region, while it is significantly more pronounced for 2.45°. e) The distance between the local minima (AA or SP) and the maximum (AB) of the moiré potential as a function of the moiré lattice constant a_M at the DFT and s-G_0W_0 level. The AB-AA curve shows a maximum for intermediate twist angles; for large a_M the AA and SP minima become practically degenerate, leading to two pronounced minima (visible in d)) when considering s-G_0W_0 results as opposed to DFT.

Table S.1. As discussed later, the one-shot corrections are sufficient to address the energies of the individual states, though they rely on the spatial distribution of the underlying KS orbitals (we address the QP state hybridization later).

From these results, we construct the effective excitonic moiré potential energy $\Delta(\mathbf{r})$ which is commonly applied to describe the twisted bilayers.[28] Here, the exciton can be described as a QP (an entangled quasi-electron and quasi-hole pair) in a potential landscape dominated by the variation of the local band gaps (assuming that the exciton binding energy is roughly constant across the system, following[28]). In contrast to the typical construction of $\Delta(\mathbf{r})$, we employ a second-order harmonic expansion to account for the SP regions in the moiré, resulting in an additional local extrema:

$$\Delta(\mathbf{r}) = V_0 + \sum_{j=1,2,3} [V_1 \cos(\mathbf{b}_j \cdot \mathbf{r}) + V_2 \cos(2\mathbf{b}_j \cdot \mathbf{r})] \quad (1)$$

Here, $|\mathbf{b}_j| = \frac{4\pi}{\sqrt{3}\, a_M}$ scales the moiré reciprocal lattice vectors where a_M is the moiré period. The constant V_0 term determines the average gap of the twisted system while the local fluctuations are captured by V_1 and V_2. Note that if only the AA and AB regions are considered (no second local minimum is present), $\Delta(\mathbf{r})$ is approximated by the lowest-order harmonic expansion.[28]

The comparison of the gap variations in the twisted structures with those obtained solely from the local environments differ significantly. The latter exaggerates the variation and the barrier heights between the distinct stacking points, as shown in Figure 1(c),(d) for the θ = 5.09° system computed with s-G_0W_0. When considering only the high-symmetry regions, the depth of the moiré valleys is overestimated by up to 0.28 and 0.13 eV and for the AA and SP regions and $\Delta(\mathbf{r})$ computed for the entire system is rather uniform with shallow valleys, affecting the overall localization of electrons and holes and, therefore, the confinement of excitons in these twisted bilayers.

Next, we investigate how the moiré potential and mutual interactions of localized states change with the twist angle and consider only the full t-hBN system. We find that decreasing the mutual twist angle does not reduce the apparent delocalization of electronic states despite the larger moiré period and increased distance between high-symmetry regions. This is somewhat surprising, as one might expect that the localized states will become more separated and effectively isolated. "Hybridization" of the high-symmetry regions, particularly in the conduction states, is clearly observed whether there is a twist angle of 5.09° or a twist angle of 2.45° (see Figure 2(a)−(d) (top)). Computed $\Delta(\mathbf{r})$ for all twist angles is shown in Figure 2(a)−(d) (bottom)). The SP valley is deeper for small twist angles (most pronounced for θ = 2.45°) and practically indistinguishable (within stochastic error) from the results for AA. In essence, the small-angle band gap landscape will show two sets of practically identical minima localized in distinct stacking regions. Depending on the twist angle, the interlayer excitons thus can be confined similarly by both AA and SP regions. While this feature is found in the many-body calculations, it is not reproduced by mean field methods.

Another surprising observation is that the barrier between SP and AB regions is highly nonmonotonic as a function of the moiré lattice constant a_M. The energy differences between AA and AB and similarly between SP and AB are shown in Figure 2(e) with maximum for intermediate angles for AA-AB. The bilayer with θ = 3.48° has the greatest variation between the different regions; it has the deepest potential in the AA region while a relatively shallow well at SP. Notably, this is associated with increased localization of electronic states in the AA region, which cannot be simply inferred from the visual inspection of the LDOS, and it is discussed below. As these effects are to a large extent driven by the nonlocal self-energy, the evaluation of $\Delta(\mathbf{r})$ with the twist angle is missed by DFT. For θ = 2.45°, DFT results show a much larger difference of the $\Delta(\mathbf{r})$ depth (i.e., the gaps at AA and SP region differ by ∼0.15 eV as opposed to ∼0.02 ± 0.04 eV with s-G_0W_0). Further, for small twist angles (a_M > 41 Å), DFT does not show a nonmonotonic dependence of the AB-AA valley barrier heights and both AA and SP minima are increasing toward

https://doi.org/10.1021/acs.nanolett.4c03030
Nano Lett. 2024, 24, 11882−11888

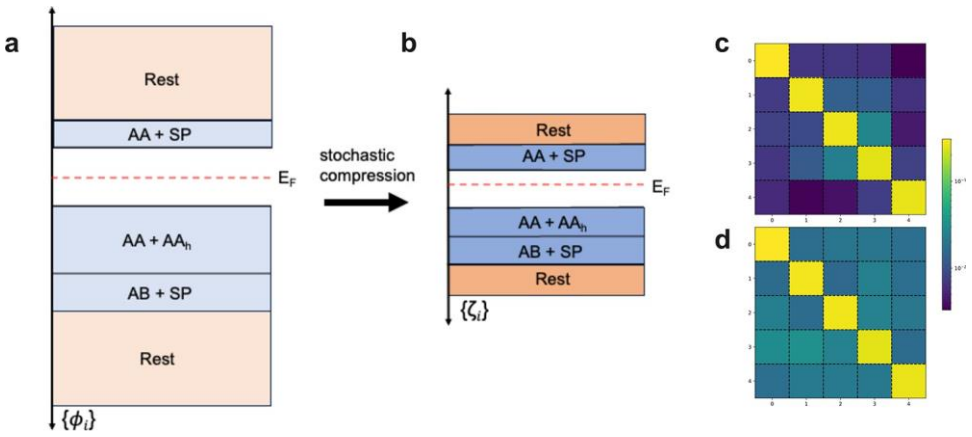

Figure 3. a) Illustration of the single-particle KS state distribution in the subspaces corresponding to the various high-symmetry stacking regions: AA, AB, SP. The AA_h region corresponds to the hybridized localization in the immediate neighborhood of AA. b) The compression of the states into a reduced dimensional representation with only five regions, among which the coupling is analyzed. c) Visualization of the full QP Hamiltonian matrix in the KS basis for the compressed states for the 3.48° twist angle that is diagonally dominant and hence localized, as in the KS picture. The rows from top to bottom and left to right represent the states of increasing energy (i.e., the top row corresponds to the block of the rest occupied states. In contrast, d) shows the QP Hamiltonian for 2.45° for which the QP states further hybridize more strongly.

small twist angles with almost constant energy offset (Figure 2(e)). It is important to note that the nonmonotonic behavior in GW for the AB-SP differences is dominated by the conduction band variation as depicted in Figure S.3. There is no AB-SP valence state energy difference due to their hybridization in the valence region, in contrast to the AB-AA valley. Moreover, comparing the DFT and GW AB-AA curves further shows that GW makes the VBM/CBM behavior more pronounced, leading to a qualitative difference in the variation of the gap (details in the SI).

To explore the coupling between different moiré states and the differences between KS and QP orbitals, we next investigated the effective QP Hamiltonian represented in the KS basis. We will focus on the role of off-diagonal self-energy terms where $\Sigma_{jk}(\omega) = \langle \phi_j | \Sigma(\omega) | \phi_k \rangle$ which mixes the KS orbitals. For the fixed-point solutions, eigenstates are the many-body Dyson orbitals that incorporate the nonlocal exchange and dynamical correlations. Given the large number of QP states (up to 8,752 occupied states) and aim to facilitate the comparison among different bilayers with a different number of total electrons, we employ a modified stochastic orbital compression technique.[43] Here, multiple orbitals are represented simultaneously by random vectors in the single-particle Hilbert space (obtained from the diagonalization of the KS Hamiltonian) selected such that they sample predetermined subspaces. This drastically reduces the computational cost and provides accurate estimates of QP energies when hybridization is involved.[43]

We chose a subspace of states that are identified through their localization in LDOS (Figure 3(a)) and sampled them by random vectors $\{\zeta\}$. We divide the system into a set of valence states that correspond to AA localization, states in the immediate neighborhood of AA (AA_h), and AB and SP hybridization as well as a set of conduction states that correspond to AA and SP hybridization. Instead of treating all of them explicitly, we construct stochastic orbitals. This compression uncovers the degree of hybridization between nearly degenerate states localized in the same stacking regions (see the SI and ref 43). This random vector basis is used to evaluate the QP Hamiltonian $H^{QP}_{jk}(\omega)$ where j and k represent state indices and the off-diagonal terms ($j \neq k$) in the random basis thus represent the coupling between the individual subspaces.

For visualization and analysis of the couplings, we averaged each component from each matrix across all 22 Hamiltonians satisfying the QP fixed-point solutions, resulting in a single 22 × 22 self-energy matrix for $\theta = 2.45°$, for instance. Due to the several degenerate states in the twisted bilayers, we perform an additional compression by averaging elements from each set of states, resulting in a (5 × 5) compressed QP Hamiltonian matrix as shown in Figure 3(c) for $\theta = 3.48°$ and Figure 3(d) for $\theta = 2.45°$, corresponding to the systems with the largest and lowest energy differences between the AA and SP $\Delta(r)$ potential minima. The basis compression for the diagonalization does not truncate the self-energy, which contains information on all the single-particle states through Green's function and the screened Coulomb interaction. Here, each block represents an averaged subspace of states containing: rest (occupied) states, AB+SP, $AA+AA_h$, AA+SP, and rest (unoccupied) states.

We find that the QP energies of H^{QP}, are mostly diagonal, and the off-diagonal eigenvalues differ only negligibly from those computed within the diagonal approximation; for instance, the maximum deviations are 1.33% difference for $\theta = 3.48°$ and 6.65% for $\theta = 2.45°$ for the localized states of interest. Therefore, the effects of the partial self-consistency in GW are small, and therefore, there should be no qualitative difference of the moiré potential when comparing these two methods. Still, we find a stark difference in the off-diagonal terms (determining the mixing of the KS states) when observing the full QP Hamiltonian matrices. Most importantly, for $\theta = 3.48°$, the QP Hamiltonian shows weaker mixing of the underlying KS states (despite some is observed across the gap in for the AA localized states indicated by lighter color of the off-diagonal block of H^{QP} in the third and fourth row/column in Figure 3(c)). These results confirm the findings for the QP energies presented above and also further strengthen the observation that systems with intermediate twist angles (here, $\theta = 3.48°$) harbor less hybridized (i.e., less delocalized) states compared to small or large twists.

In conclusion, by studying the near-gap electronic states and band gap variations in t-hBN, we uncovered how the electronic

https://doi.org/10.1021/acs.nanolett.4c03030
Nano Lett. 2024, 24, 11882−11888

structure of large-scale twisted structures depends on the underlying nonlocal interactions. The local gap variation (associated with the excitonic potential) cannot be simply generated by considering only local environments. The latter leads to a gross exaggeration of the features and spuriously suggests a strong confinement of excitons in only one region. There also exists a nontrivial interplay of correlations between the monolayers, which significantly reduces the energy barriers between the valleys of the excitonic potential. For large twist angles, the small moiré unit cells lead to strong hybridization of the localized states and rather uniform band gap variation. At small twist angles, the correlation effects weaken but the energy barriers are much smaller, again leading to delocalization of electronic states across the high-symmetry regions. Surprisingly, there is an intermediate twist angle regime at $\theta = 3.48°$ at which the energy separation barriers between the individual localized states are large. We surmise that for such angles the QPs localization may not need to be assisted by phonons or lattice distortions. Further, we find that the moire potential hosts two minima in distinct stacking regions (which become practically degenerate for small twist angles) that can host two types of moire excitons. Besides addressing the QP properties discussed in this work, the methodology allows the development of accurate *ab initio* model Hamiltonians like tight-binding models to describe electronic, excitonic,[28] magnetic properties,[58] and other rich physics related to the strong correlations.[52,59,60] These models have so far heavily relied on the analysis of first-principles calculations based solely on the local environments. We believe this is an important stepping stone for reevaluating how we treat moiré superlattices, allowing for a more direct comparison to experiments.

■ ASSOCIATED CONTENT

Supporting Information

The Supporting Information is available free of charge at https://pubs.acs.org/doi/10.1021/acs.nanolett.4c03030.

Computational details, stochastic many-body theory, band gap data, moiré potential fit, LDOS plots, self-energy Hamiltonian (PDF)

■ AUTHOR INFORMATION

Corresponding Author

Vojtěch Vlček – *Materials Department and Department of Chemistry and Biochemistry, University of California, Santa Barbara, California 93106-9510, United States*; Email: vlcek@ucsb.edu

Authors

Arsineh Apelian – *Materials Department, University of California, Santa Barbara, California 93106-9510, United States*; orcid.org/0000-0002-3713-5043

Annabelle Canestraight – *Department of Chemical Engineering, University of California, Santa Barbara, California 93106-9510, United States*; orcid.org/0000-0001-6473-3762

Songyuan Liu – *Department of Physics, University of California, Santa Barbara, California 93106-9510, United States*

Complete contact information is available at: https://pubs.acs.org/10.1021/acs.nanolett.4c03030

Notes

The authors declare no competing financial interest.

■ ACKNOWLEDGMENTS

The authors thank Barak Hirshberg and Netanel Bachar Schwartz at Tel Aviv University for their fruitful discussions. The methodological development, selected simulations for the large-scale systems, and the analysis were supported by the National Science Foundation (NSF) CAREER award through grant no. DMR-1945098. We acknowledge funding from the UC Office of the President within the Multicampus Research Programs and Initiatives (M23PR5931) supporting some of the calculations performed in this work. The work on model moiré potentials was supported by the United States - Israel Binational Science Foundation (contract no. 2020083). Use was made of computational facilities purchased with funds from the NSF (CNS-1725797) and administered by the Center for Scientific Computing (CSC). The CSC is supported by the California NanoSystems Institute and the Materials Research Science and Engineering Center (MRSEC; NSF DMR 2308708) at UC Santa Barbara. A.A. was supported by the NSF Graduate Research Fellowship under Grant No. (2139319).

■ REFERENCES

(1) Schaibley, J. R.; Yu, H.; Clark, G.; Rivera, P.; Ross, J. S.; Seyler, K. L.; Yao, W.; Xu, X. Valleytronics in 2D Materials. *Nat. Rev. Mater.* 2016, *1*, 16055.

(2) Pan, Y.; Fölsch, S.; Nie, Y.; Waters, D.; Lin, Y.; Jariwala, B.; Zhang, K.; Cho, K.; Robinson, J. A.; Feenstra, R. M. Quantum-Confined Electronic States Arising from the Moiré Pattern of MoS2−WSe2 Heterobilayers. *Nano Lett.* 2018, *18*, 1849−1855.

(3) Yankowitz, M.; Ma, Q.; Jarillo-Herrero, P.; LeRoy, B. J. Van der Waals Heterostructures Combining Graphene and Hexagonal Boron Nitride. *Nat. Rev. Phys.* 2019, *1*, 112−125.

(4) Zheng, Z.; et al. Unconventional Ferroelectricity in Moiré Heterostructures. *Nature* 2020, *588*, 71−76.

(5) Leconte, N.; Jung, J. Commensurate and Incommensurate Double Moire Interference in Graphene Encapsulated by Hexagonal Boron Nitride. *2D Materials* 2020, *7*, 031005.

(6) Wu, S.; Killi, M.; Paramekanti, A. Graphene Under Spatially Varying External Potentials: Landau levels, Magnetotransport, and Topological Modes. *Phys. Rev. B* 2012, *85*, 195404.

(7) Yankowitz, M.; Xue, J.; Cormode, D.; Sanchez-Yamagishi, J. D.; Watanabe, K.; Taniguchi, T.; Jarillo-Herrero, P.; Jacquod, P.; LeRoy, B. J. Emergence of Superlattice Dirac Points in Graphene on Hexagonal Boron Nitride. *Nat. Phys.* 2012, *8*, 382−386.

(8) van der Zande, A. M.; Kunstmann, J.; Chernikov, A.; Chenet, D. A.; You, Y.; Zhang, X.; Huang, P. Y.; Berkelbach, T. C.; Wang, L.; Zhang, F.; Hybertsen, M. S.; Muller, D. A.; Reichman, D. R.; Heinz, T. F.; Hone, J. C. Tailoring the Electronic Structure in Bilayer Molybdenum Disulfide via Interlayer Twist. *Nano Lett.* 2014, *14*, 3869−3875.

(9) Cao, Y.; Fatemi, V.; Fang, S.; Watanabe, K.; Taniguchi, T.; Kaxiras, E.; Jarillo-Herrero, P. Unconventional superconductivity in magic-angle graphene superlattices. *Nature* 2018, *556*, 43−50.

(10) Hunt, B.; Sanchez-Yamagishi, J. D.; Young, A. F.; Yankowitz, M.; LeRoy, B. J.; Watanabe, K.; Taniguchi, T.; Moon, P.; Koshino, M.; Jarillo-Herrero, P.; Ashoori, R. C. Massive Dirac Fermions and Hofstadter Butterfly in a van der Waals Heterostructure. *Science* 2013, *340*, 1427−1430.

(11) Kim, K.; DaSilva, A.; Huang, S.; Fallahazad, B.; Larentis, S.; Taniguchi, T.; Watanabe, K.; LeRoy, B. J.; MacDonald, A. H.; Tutuc, E. Tunable Moiré Bands and Strong Correlations in Small-Twist-Sngle Bilayer Graphene. *Proc. Natl. Acad. Sci. U.S.A* 2017, *114*, 3364−3369.

(12) Dean, C. R.; Wang, L.; Maher, P.; Forsythe, C.; Ghahari, F.; Gao, Y.; Katoch, J.; Ishigami, M.; Moon, P.; Koshino, M.; Taniguchi, T.; Watanabe, K.; Shepard, K. L.; Hone, J.; Kim, P. Hofstadter's Butterfly and the Fractal Quantum Hall Effect in Moiré Superlattices. *Nature* 2013, *497*, 598−602.
(13) Xian, L.; Kennes, D. M.; Tancogne-Dejean, N.; Altarelli, M.; Rubio, A. Multiflat Bands and Strong Correlations in Twisted Bilayer Boron Nitride: Doping-Induced Correlated Insulator and Superconductor. *Nano Lett.* 2019, *19*, 4934−4940.
(14) Zhao, X.-J.; Yang, Y.; Zhang, D.-B.; Wei, S.-H. Formation of Bloch Flat Bands in Polar Twisted Bilayers without Magic Angles. *Phys. Rev. Lett.* 2020, *124*, 086401.
(15) Roman-Taboada, P.; Obregon-Castillo, E.; Botello-Mendez, A. R.; Noguez, C. Excitons in twisted AA′ hexagonal boron nitride bilayers. *Phys. Rev. B* 2023, *108*, 075109.
(16) Devakul, T.; Crépel, V.; Zhang, Y.; Fu, L. Magic in twisted transition metal dichalcogenide bilayers. *Nat. Commun.* 2021, *12*, 6730.
(17) Wang, L.; et al. Correlated electronic phases in twisted bilayer transition metal dichalcogenides. *Nat. Mater.* 2020, *19*, 861−866.
(18) Tang, B.; Che, B.; Xu, M.; Ang, Z. P.; Di, J.; Gao, H.-J.; Yang, H.; Zhou, J.; Liu, Z. Recent Advances in Synthesis and Study of 2D Twisted Transition Metal Dichalcogenide Bilayers. *Small Structures* 2021, *2*, 2000153.
(19) Wu, F.; Lovorn, T.; Tutuc, E.; Martin, I.; MacDonald, A. H. Topological Insulators in Twisted Transition Metal Dichalcogenide Homobilayers. *Phys. Rev. Lett.* 2019, *122*, 086402.
(20) Zhan, Z.; Zhang, Y.; Lv, P.; Zhong, H.; Yu, G.; Guinea, F.; Silva-Guillén, J. A.; Yuan, S. Tunability of multiple ultraflat bands and effect of spin-orbit coupling in twisted bilayer transition metal dichalcogenides. *Phys. Rev. B* 2020, *102*, 241106.
(21) Su, H.; Xu, D.; Cheng, S.-W.; Li, B.; Liu, S.; Watanabe, K.; Taniguchi, T.; Berkelbach, T. C.; Hone, J. C.; Delor, M. Dark-Exciton Driven Energy Funneling into Dielectric Inhomogeneities in Two-Dimensional Semiconductors. *Nano Lett.* 2022, *22*, 2843−2850.
(22) Chan, Y.-h.; Naik, M. H.; Haber, J. B.; Neaton, J. B.; Louie, S. G.; Qiu, D. Y.; da Jornada, F. H. Exciton−Phonon Coupling Induces a New Pathway for Ultrafast Intralayer-to-Interlayer Exciton Transition and Interlayer Charge Transfer in WS2-MoS2 Heterostructure: A First-Principles Study. *Nano Lett.* 2024, *24*, 7972−7978.
(23) Brooks, J.; Weng, G.; Taylor, S.; Vlček, V. Stochastic Many-Body Perturbation Theory for Moiré States in Twisted Bilayer Phosphorene. *J. Phys.: Condens. Matter* 2020, *32*, 234001.
(24) Soltero, I.; Guerrero-Sánchez, J.; Mireles, F.; Ruiz-Tijerina, D. A. Moiré band structures of twisted phosphorene bilayers. *Phys. Rev. B* 2022, *105*, 235421.
(25) Zhao, S.; Wang, E.; Uzer, E. A.; Guo, S.; Qi, R.; Tan, J.; Watanabe, K.; Taniguchi, T.; Nilges, T.; Gao, P.; et al. Anisotropic moiré optical transitions in twisted monolayer/bilayer phosphorene heterostructures. *Nat. Commun.* 2021, *12*, 3947.
(26) Ud Din, N.; Liu, Z.-F. Anisotropy of the Optical Properties of Pentacene:Black Phosphorus Interfaces. *J. Phys. Chem. C* 2022, *126*, 20694−20701.
(27) Yoon, S.; Kim, T.; Seo, S.-Y.; Shin, S.-H.; Song, S.-B.; Kim, B. J.; Watanabe, K.; Taniguchi, T.; Lee, G.-H.; Jo, M.-H.; et al. Electrical control of anisotropic and tightly bound excitons in bilayer phosphorene. *Phys. Rev. B* 2021, *103*, L041407.
(28) Wu, F.; Lovorn, T.; MacDonald, A. H. Theory of Optical Absorption by Interlayer Excitons in Transition Metal Dichalcogenide Heterobilayers. *Phys. Rev. B* 2018, *97*, 035306.
(29) Wu, F.; Qu, F.; MacDonald, A. H. Exciton Band Structure of Monolayer MoS_2. *Phys. Rev. B* 2015, *91*, 075310.
(30) Guo, H.; Zhang, X.; Lu, G. Shedding Light on Moiré Excitons: A First-Principles Perspective. *Science Advances* 2020, *6*, eabc5638.
(31) Zhang, Y.; Yuan, N. F. Q.; Fu, L. Moiré Quantum Chemistry: Charge transfer in Transition Metal Dichalcogenide Superlattices. *Phys. Rev. B* 2020, *102*, 201115.
(32) Tran, K.; Moody, G.; Wu, F.; et al. Evidence for Moiré Excitons in van der Waals Heterostructures. *Nature* 2019, *567*, 71−75.
(33) Seyler, K. L.; Rivera, P.; Yu, H.; Wilson, N. P.; Ray, E. L.; Mandrus, D. G.; Yan, J.; Yao, W.; Xu, X. Signatures of Moiré-trapped Valley Excitons in MoSe2/WSe2 Heterobilayers. *Nature* 2019, *567*, 66−70.
(34) Jin, C.; Regan, E. C.; Yan, A.; Iqbal Bakti Utama, M.; Wang, D.; Zhao, S.; Qin, Y.; Yang, S.; Zheng, Z.; Shi, S.; Watanabe, K.; Taniguchi, T.; Tongay, S.; Zettl, A.; Wang, F. Observation of Moiré Excitons in WSe2/WS2 Heterostructure Superlattices. *Nature* 2019, *567*, 76−80.
(35) Tartakovskii, A. Excitons in 2D Heterostructures. *Nat. Rev. Phys.* 2020, *2*, 8−9.
(36) Li, H.; et al. Imaging Moiré Flat Bands in Three-dimensional Reconstructed WSe2/WS2 Superlattices. *Nat. Mater.* 2021, *20*, 945−950.
(37) Naik, M. H.; Jain, M. Ultraflatbands and Shear Solitons in Moiré Patterns of Twisted Bilayer Transition Metal Dichalcogenides. *Phys. Rev. Lett.* 2018, *121*, 266401.
(38) Susarla, S.; Naik, M. H.; Blach, D. D.; Zipfel, J.; Taniguchi, T.; Watanabe, K.; Huang, L.; Ramesh, R.; da Jornada, F. H.; Louie, S. G.; Ercius, P.; Raja, A. Hyperspectral Imaging of Exciton Confinement within a Moiré Unit Cell with a Subnanometer Electron Probe. *Science* 2022, *378*, 1235−1239.
(39) Naik, M. H.; et al. Intralayer Charge-Transfer Moiré Excitons in van der Waals Superlattices. *Nature* 2022, *609*, 52−57.
(40) Romanova, M.; Vlček, V. Stochastic Many-body Calculations of Moiré States in Twisted Bilayer Graphene at High Pressures. *npj Comput. Mater.* 2022, *8*, 11.
(41) Vlček, V.; Li, W.; Baer, R.; Rabani, E.; Neuhauser, D. Swift GW Beyond 10,000 Electrons Using Sparse Stochastic Compression. *Phys. Rev. B* 2018, *98*, 075107.
(42) Vlček, V.; Rabani, E.; Neuhauser, D.; Baer, R. Stochastic GW Calculations for Molecules. *J. Chem. Theory Comput.* 2017, *13*, 4997−5003.
(43) Canestraight, A.; Lei, X.; Ibrahim, K. Z.; Vlček, V. Efficient Quasiparticle Determination beyond the Diagonal Approximation via Random Compression. *J. Chem. Theory Comput.* 2024, *20*, 551−557.
(44) He, Z.; Sun, A.-A.; Gao, S.-P. Electron-phonon scattering and stacking sequences in hexagonal boron nitride: An ab initio study. *Phys. Rev. B* 2023, *108*, 165108.
(45) Roux, S.; Arnold, C.; Carré, E.; Plaud, A.; Ren, L.; Janzen, E.; Edgar, J. H.; Maestre, C.; Toury, B.; Journet, C.; Garnier, V. et al. Exciton Self-Trapping in Twisted Hexagonal Boron Nitride Homostructures. *arXiv (Materials Science)*, May 15, 2024, arXiv:2405.09420. DOI: 10.48550/arXiv.2405.09420 (accessed May 18, 2024).
(46) Cassabois, G.; Valvin, P.; Gil, B. Hexagonal Boron Nitride is an Indirect Bandgap Semiconductor. *Nat. Photonics* 2016, *10*, 262−266.
(47) Xiao, D.; Liu, G.-B.; Feng, W.; Xu, X.; Yao, W. Coupled Spin and Valley Physics in Monolayers of MoS_2 and Other Group-VI Dichalcogenides. *Phys. Rev. Lett.* 2012, *108*, 196802.
(48) Mak, K. F.; He, K.; Shan, J.; Heinz, T. F. Control of Valley Polarization in Monolayer MoS−2 by Optical Helicity. *Nat. Nanotechnol.* 2012, *7*, 494−498.
(49) Zeng, H.; Dai, J.; Yao, W.; Xiao, D.; Cui, X. Valley Polarization in MoS_2 Monolayers by Optical Pumping. *Nat. Nanotechnol.* 2012, *7*, 490−493.
(50) Cao, T.; Wang, G.; Han, W.; Ye, H.; Zhu, C.; Shi, J.; Niu, Q.; Tan, P.; Wang, E.; Liu, B.; Feng, J. Valley-Selective Circular Dichroism of Monolayer Molybdenum Disulphide. *Nat. Commun.* 2012, *3*, 887.
(51) Jones, A. M.; Yu, H.; Ghimire, N. J.; Wu, S.; Aivazian, G.; Ross, J. S.; Zhao, B.; Yan, J.; Mandrus, D. G.; Xiao, D.; Yao, W.; Xu, X. Optical Generation of Excitonic Valley Coherence in Monolayer WSe_2. *Nat. Nanotechnol.* 2013, *8*, 634−638.
(52) Bennett, D.; Larson, D. T.; Sharma, L.; Carr, S.; Kaxiras, E. Twisted bilayer graphene revisited: Minimal two-band model for low-energy bands. *Phys. Rev. B* 2024, *109*, 155422.

https://doi.org/10.1021/acs.nanolett.4c03030
Nano Lett. 2024, 24, 11882−11888

(53) Mucha-Kruczyński, M.; Aleiner, I. L.; Fal'ko, V. I. Strained bilayer graphene: Band structure topology and Landau level spectrum. *Phys. Rev. B* 2011, *84*, 041404.
(54) Cantele, G.; Alfè, D.; Conte, F.; Cataudella, V.; Ninno, D.; Lucignano, P. Structural relaxation and low-energy properties of twisted bilayer graphene. *Phys. Rev. Res.* 2020, *2*, 043127.
(55) Zhao, X.-J.; Yang, Y.; Zhang, D.-B.; Wei, S.-H. Formation of Bloch Flat Bands in Polar Twisted Bilayers without Magic Angles. *Phys. Rev. Lett.* 2020, *124*, 086401.
(56) Watanabe, K.; Taniguchi, T.; Kanda, H. Direct-bandgap Properties and Evidence For Ultraviolet Lasing of Hexagonal Boron Nitride Single Crystal. *Nat. Mater.* 2004, *3*, 404−409.
(57) Paleari, F.; Galvani, T.; Amara, H.; Ducastelle, F.; Molina-Sánchez, A.; Wirtz, L. Excitons in Few-Layer Hexagonal Boron Nitride: Davydov Splitting and Surface Localization. *2D Materials* 2018, *5*, 045017.
(58) Yang, Y.; Morales, M. A.; Zhang, S. Metal-Insulator Transition in a Semiconductor Heterobilayer Model. *Phys. Rev. Lett.* 2024, *132*, 076503.
(59) Lu, J. Z.; Zhu, Z.; Angeli, M.; Larson, D. T.; Kaxiras, E. Low-energy moiré phonons in twisted bilayer van der Waals heterostructures. *Phys. Rev. B* 2022, *106*, 144305.
(60) Morales-Durán, N.; Potasz, P.; MacDonald, A. H. Magnetism and Quantum Melting in Moiré-material Wigner crystals. *Phys. Rev. B* 2023, *107*, 235131.

https://doi.org/10.1021/acs.nanolett.4c03030
Nano Lett. 2024, 24, 11882−11888